Check for updates

View Article Online
View Journal

Metallomics

Integrated biometal science

Accepted Manuscript

This article can be cited before page numbers have been issued, to do this please use: L. M. Balsa, P. Quispe, E. J. Baran, M. Lavecchia and I. Leon, *Metallomics*, 2020, DOI: 10.1039/D0MT00176G.

This is an Accepted Manuscript, which has been through the Royal Society of Chemistry peer review process and has been accepted for publication.

Accepted Manuscripts are published online shortly after acceptance, before technical editing, formatting and proof reading. Using this free service, authors can make their results available to the community, in citable form, before we publish the edited article. We will replace this Accepted Manuscript with the edited and formatted Advance Article as soon as it is available.

You can find more information about Accepted Manuscripts in the Information for Authors.

Please note that technical editing may introduce minor changes to the text and/or graphics, which may alter content. The journal's standard Terms & Conditions and the Ethical guidelines still apply. In no event shall the Royal Society of Chemistry be held responsible for any errors or omissions in this Accepted Manuscript or any consequences arising from the use of any information it contains.

ROYAL SOCIETY OF CHEMISTRY

rsc.li/metallomics

View Article Online
DOI: 10.1039/D0MT00176G

Significance to metallomics

The impact of dilucidation of molecular targets involved in anticancer and antimetastatic effects of novel metal based drugs is now emerging as a critical point on the drug discovery. It has been demonstrated based on in silico and in vitro studies, the mechanism of inhibition of Focal Adhesion Kinase (FAK) by $VO(CQ)_2$ and the relationship with the antitumor and anti-migration properties on a human osteosarcoma cell line (MG-63).

Published on 14 October 2020. Downloaded by Auckland University of Technology on 10/26/2020 7:34:17 PM.

Metallomics Accepted Manuscript

View Article Online
DOI: 10.1039/D0MT00176G

In silico and in vitro analysis of FAK/MMP signaling axis inhibition by VO-clioquinol on 2D and 3D human osteosarcoma cancer cells

Lucia M. Balsa [1], Patricia Quispe [1], Enrique J. Baran [1], Martin J. Lavecchia *[1], Ignacio E. León*[1]

[1] Centro de Química Inorgánica (CEQUINOR, CONICET-UNLP), Facultad de Ciencias Exactas, Universidad Nacional de La Plata, Bv 120 1465, 1900 La Plata, Argentina

* Corresponding author: ileon@biol.unlp.edu.ar , lavecchia@quimica.unlp.edu.ar

Published on 14 October 2020. Downloaded by Auckland University of Technology on 10/26/2020 7:34:17 PM.

Abstract

The study of novel mechanism of action of vanadium compounds is critical to dilucidated the role and importance of these kind of compounds as antitumor and antimetastatic agents. This work deals with in silico and in vitro studies of one clioquinol oxidovanadium(IV) complex [$VO(clioquinol)_2$], $VO(CQ)_2$, and its regulation over FAK. In particular, we focus in elucidate the relationship in the FAK inhibition, MMPs activity and the antimetastatic effects of complex on human bone cancer cells.

1. Introduction

Vanadium is an ultratrace element present in higher plants and animals [1]. The therapeutic actions of vanadium convert its compounds into possible pharmaceutics agents to be used in the treatments of different pathologies, including neurodegenerative diseases, diabetes, and cancer.[2] In this sense, the anticancer activity of vanadium compounds has been widely investigated on various types of cancer cell lines such us breast, colorectal, bone, lung, among others. [3–5] Taking into account, that great amounts of vanadium are detected in bones,[1] the antitumor properties of many vanadium complexes has been broadly explored against osteosarcoma cells. [6–8] Therefore, vanadium compounds have recently emerged as non-platinum antitumor agents. [9] Nevertheless, a few challenges remain for their uses and application of this kind of compounds, such as lack of specificity, poor absorption, unknown mechanism of action, among others. In this order, the study of cell signaling pathways regulated by vanadium complexes is required for the discovery of new mechanism of action for the treatment of cancer. Previously, we demonstrated that

Metallomics Accepted Manuscript

View Article Online
DOI: 10.1039/D0MT00176G

Published on 14 October 2020. Downloaded by Auckland University of Technology on 10/26/2020 7:34:17 PM.

vanadium-chrysin and vanadium-clioquinol complexes inhibit the activation of Focal Adhesion Kinase (FAK) decreasing the cell proliferation in human osteosarcoma cells [10,11]. Particularly, our results showed that vanadium-clioquinol exhibits a dual behavior since at 2.5 μM up-regulated Tyr576 and Tyr577 sites but at 10 μM the phosphorylation of Tyr576 and Tyr577 decreased 14-fold [11]. Moreover, ruthenium-based inhibitors have been developed in the last few years and crystallized in the Adenosine triphosphate (ATP) binding site of a different protein kinases [12–15].

On the other hand, FAK is a tyrosine kinase which plays a key role in adhesion, survival, motility, angiogenesis and metastasis of cancer cells [16]. Besides, FAK is overexpressed in many types of solid and non–solid tumors [17] so FAK was proposed as a therapeutic target [18].

In recent years, several strategies have been developed to interfere with the expression and activation of FAK. [19] In this context, decoding the mode of interaction of vanadium compounds with FAK and related to the anti-migration and anti-invasion properties is of great interest.

In literature, inhibitors of the ATP site of FAK have been reported, reducing phosphorylation in the residue Tyr397. TAE-226, PF-562,271, and 10N are examples of this class of inhibitors [20] [21] [22] and they have been crystallized in the ATP site. This is a previous step in the activation cascade of FAK by Src, responsible for the phosphorylation of Tyr 576/577 [23].

In addition, clioquinol is an FDA-approved topical antifungal agent that the chemical composition is 5-chloro-7-iodo-8-quinolinol. This drug were proposed to the repurposing proposes but these efforts were not successful since very low intracellular leves of clioquinol is appear into the cells. Therefore, many research approaches focus on chelate the clioquinol with several metals to improve its poor absorption and pharmacological activities [24].

As part of a project, this research deals with the deciphering of mode of interaction between one oxidovanadium(IV) complex with clioquinol [$VO(clioquinol)_2$], **$VO(CQ)_2$**, (see Figure 1) and FAK. In particular, the present study mainly focused to elucidate the relationship in the FAK regulation, Matrix metalloproteinases (MMPs) activity and the antimetastatic effects of complex on 2D and 3D human osteosarcoma cell models.

2. Results and discussion

Metallomics Accepted Manuscript

View Article Online
DOI: 10.1039/D0MT00176G

Published on 14 October 2020. Downloaded by Auckland University of Technology on 10/26/2020 7:34:17 PM.

Based in our previous results [11] and with the aim of elucidate the mode of interaction between **VO(CQ)$_2$** and FAK on Tyr576 and Tyr577 residues[11], computational studies were performed, including Molecular Docking and Molecular Dynamics.

2.1 Docking results

Molecular docking was performed in the ATP binding site of the FAK Kinase Domain under the hypothesis that a possible interaction in this region could lead to inhibition of its activation. It should be noted that in the literature there are several examples of metal complexes designed to establish binding interactions with residues surrounding the ATP binding site of kinases [12].

In order to evaluate the performance of docking protocol using AutoDock 4.2 (see Methodology) , three inhibitors co-crystallized with FAK: 2-[[5-chloro-2-(2-methoxy-4-morpholin-4-ylanilino)pyrimidin-4-yl]amino]-N-methylbenzamide(TAE-226, PDB Id 2JKK), N-methyl-N-[3-[[[2-[(2-oxo-1,3-dihydroindol-5-yl)amino]-5-(trifluoromethyl)-4-pyrimidinyl]amino]methyl]-2-pyridinyl]methanesulfonamide (PF-562,271, PDB Id 3BZ3), and N-{3-[(5-Cyano-2-phenyl-1H-pyrrolo[2,3-b]pyridin-4-ylamino)- methyl]-pyridin-2-yl}-N-methyl-methanesulfonamide (10N, PDB Id 4GU6), which are shown in Figure 1, were redocked into the ATP binding site of FAK. The resulting poses were compared with the native conformations in the crystal structure, exhibiting a root mean square deviation (RMSD) of 0.689 Å, 1.181 Å and 1.204 Å respectively (Figure 2). A value of RMSD less than 2 Å between the docking pose and the experimental conformation can be taken as criteria of a good performance of the docking methodology[25,26], so these results confirm the accuracy of the AutoDock 4.2 software for this study. In general, the agreement was good except for methanesulfonamide group orientation of 10N, which is rotated with respect to the experimental structure.

The **VO(CQ)$_2$** structure was modeled with Density-functional theory (DFT) and then, it was docked following same protocol used for the previously mentioned inhibitors. A unique conformational cluster was obtained, presenting a -4.94 kcal/mol score value, and whose resulting binding mode of **VO(CQ)$_2$** is depicted in Figure 3a. The complex is located near of the activation loop of the kinase domain and establishes interactions with residues of binding site.

Metallomics Accepted Manuscript

View Article Online
DOI: 10.1039/D0MT00176G

In addition, the proposed location of **VO(CQ)$_2$** was compared with a crystallized ruthenium complex [13] in another kinase, Glycogen Synthase Kinase 3. For this purpose, ATP sites of both protein structures were aligned and metal center locations were compared. Figure 3b shows this comparison, where it is observed that the transition-metal atoms are located in the same region.

2.2 Molecular Dynamics and Binding Energies

Molecular Dynamics (MD) simulation studies were then performed to investigate stability of **VO(CQ)$_2$** in the ATP binding site and to explore further the interactions established with residues. The poses of **VO(CQ)$_2$** and the three inhibitors obtained by docking were selected and submitted to a MD with a minimization, heating and follow for a 40 ns of equilibration/production period.

RMSD plots (Figure SM1) show that both the ligands (**PF-562,271**, **TAE-226**, **10N**, and **VO(CQ)$_2$**) and FAK Kinase Domain reach stabilization during molecular dynamic simulations.

Molecular Mechanics/Generalized Born Surface Area (MM-GBSA) binding energies were (in kcal/mol, standard deviation in parenthesis), **TAE-226**: -46.8 (3.2), **PF-562,271**: -46.7 (2.3), **10N**: -44.9 (2.9), **VO(CQ)$_2$**: 1.90 (11.7). These results, taking into account the value and standard deviation, do not correlate with the greater stability of **VO(CQ)$_2$** shown during the DM trajectory (see RMSD plots, Figure SM1).

With the intention of establishing a more reliable interaction energy, semi-empirical calculations were performed with the PM7 method, implemented in MOPAC. These calculations were made with the MOZYME approach, which allows treating large systems such as proteins. Binding enthalpies were calculated as HOF(complex)-HOF (ligand)-HOF(protein), where HOF is the heat of formation of the most probable conformation during the MD trajectory. It was found that the order of stability was **TAE-226** > **PF-562,271** > **VO(CQ)$_2$** > **10N**. However, this result should be taken with caution, since the evaluation is on a single conformation, and despite including electronic effects, vanadium is a transition metal which generally increases errors in calculations of this type.

Despite the limitations that the MM-GBSA method may have for treating transition metals, as it was implemented for **VO(CQ)$_2$**, we believe that it can be useful to analyze the interactions with FAK residues.

Published on 14 October 2020. Downloaded by Auckland University of Technology on 10/26/2020 7:34:17 PM.

Metallomics Accepted Manuscript

View Article Online
DOI: 10.1039/D0MT00176G

Published on 14 October 2020. Downloaded by Auckland University of Technology on 10/26/2020 7:34:17 PM.

VO(CQ)$_2$ localization can be appreciated in Figure 4. It is observed that there were no major changes with respect to the pose obtained by docking.

Binding free energy decomposition by residue analysis allowed to identify the residues Ile428, Leu501, Cys502, Gly505, Glu506, Asn551, Leu553, Gly563, Asp564, and Leu567 whose contribution to the total interaction energy under molecular mechanics energies combined with the generalized Born and surface area continuum solvation MM-GB/SA model was significant for reference inhibitors. In addition, most of these residues are important for interaction with **VO(CQ)$_2$** (histograms and a detailed description of the interactions are shown in Figure 5 and Table SM1, respectively). It should be noted that for reference inhibitors these results are in agreement with what has been experimentally observed, also, interaction pattern is remarkably similar for the three reference inhibitors. Besides, **TAE-226** has already been studied computationally by Zhan et al [27] and our results coincide with those reported in this scientific reports. Moreover, **VO(CQ)$_2$** presents similar interactions to those described for the reference inhibitors: quinoline rings moieties which establish hydrophobic contacts with the side chains of Ile428, Leu501, Gly505, Glu506, Leu553 and Leu567. These residues provide the same type of interaction with reference inhibitors. An additional carbon hydrogen bond is established between the carbonyl group of Ile428 and a quinoline ring, which increases the magnitude of interaction with this residue. Unlike reference inhibitors, a halogen bond interaction is established between the carbonyl group of Cys502 with a chlorine atom of **VO(CQ)$_2$**. The carbonyl group of Asn551 establishes a carbon hydrogen bond interaction with a pyridine ring, same interaction type established by reference inhibitors with this residue. On the other hand, **VO(CQ)$_2$** does not establish interactions of significant magnitude with residues Gly563 and Asp564. This last residue exhibits for the three reference inhibitors studied in this work an important interaction by hydrogen bond, although this is not a fundamental condition for FAK inhibition. 7-(pyridin-2-yl)-N-(3,4,5-trimethoxyphenyl)-7H-pyrrolo[2,3-d]pyrimidin-2-amine inhibitors, which was crystallized and computationally studied, did not show an appreciable interaction with this residue [27].

In addition, **VO(CQ)$_2$** shows interactions *w*ith Tyr570 and Lys581, that were not observed for *r*eference inhibitors. These residues, which are part of the activation loop, are located far from the ATP binding pocket and undergo a displacement during MD simulation, see Figure 4. Tyr570 residue establishes van der Waals interaction with a quinoline ring system of **VO(CQ)$_2$** complex and this is maintained during the trajectory. Lys581 also establishes both van der Waals and cation-π interactions with a quinoline

Metallomics Accepted Manuscript

View Article Online
DOI: 10.1039/D0MT00176G

Published on 14 October 2020. Downloaded by Auckland University of Technology on 10/26/2020 7:34:17 PM.

ring system of **VO(CQ)$_2$** complex, which are maintained during the last 10 ns. There is not information in literature that supports a potential biological relevance of Tyr570 residue. Moreover, Lys581 residue appears to have a certain biological relevance, as was previously reported by Gabarra-Niecko *et al* [28], showing that the double substitution of lysine residues (Lys578 and Lys581) with glutamic acid residues leads to a FAK hyperactivation state and, in consequence, biochemical and cellular events regulated by it were increased.

2.3 Synthesis and characterization of VO(CQ)$_2$

VO(CQ)$_2$ was synthesized according to our previous results [29]. The structure of the compound has been proposed on the basis of elemental analysis, Nuclear Magnetic Resonance (NMR), and Infrared (IR) spectroscopy.

2.4 Effect of VO(CQ)$_2$ on cell migration

Cell migration is an important feature of live cells and crucial for normal growth, and disease developments including cancer metastasis and inflammation. [30]

The study of cell migration in cancer research is of great interest since many patient's death due to metastatic progression. In this context, is relevant to highlight the role of FAK in MG-63 cell migration and pharmacological importance related to FAK inhibition. So, we evaluated the effect of **VO(CQ)$_2$** on cell migration (wound healing assay) on bone cancer cells. Figure 6 showed that compound interfere with the cell migration of MG-63 cells from 2.5 to 10 μM. As it can be seen, that **VO(CQ)$_2$** inhibited cell migration of bone cancer cells by 58% (2.5 μM) and 51% (10 μM), compared to 68% in untreated cells ($p < 0.01$). Some oxidovanadium(IV) compounds inhibit the cell migration of human cancer cells including stomach [31], prostate [32], bone [33], breast and colorectal. [34]

2.5 Effect of VO(CQ)$_2$ on MMP-2 and MMP-9 activity

Matrix metalloproteinases are proteolytic enzymes that show a key role in extracellular matrix (ECM) remodeling but have also been shown to be involved in the regulation of multiple stages of cancer progression and metastasis.[35] In this way, higher MMP levels have been shown to be associated with metastasis and poor prognosis in different kind of

Metallomics Accepted Manuscript

View Article Online
DOI: 10.1039/D0MT00176G

Published on 14 October 2020. Downloaded by Auckland University of Technology on 10/26/2020 7:34:17 PM.

solid tumors. [36] Moreover, MMPs play an important role in the degradation of the ECM and promote the angiogenesis inducing the release of proangiogenic factors such us, vascular endothelial growth factor (VEGF) and Transforming growth factor beta (TGF-ß) from the ECM. [37]

We used gelatin zymography to investigate the effect of **$VO(CQ)_2$** on MG-63 cell MMP-2 and MMP-9 enzymes activity.

As shown in Figure 7, **$VO(CQ)_2$** significantly reduced the activity of MMP-2 and MMP-9 in MG-63 cells in a dose-dependent manner ($p<0.01$). The incubation of the cells with 2.5, 5 and 10 μM of complex significantly reduced MMP-2 and MMP-9 activity compared with untreated cells. In this sense, Narla et al published that [bis(4,7-dimethyl-1,10 phenanthroline) sulfatooxovanadium(IV) (0.5-2 μM) diminished the level and actions of MMP-2 and MMP-9 proteins on primary leukemic cells [4]. Moreover, Petanidis et al reported that V(V)-peroxido-betaine compound reduced MMP-2 levels on breast and lung cancer cells but in higher concentrations (100-300 μM) [38].

In this order, Kunz *et al*. report that elevated ratio of MMP-2/MMP-9 is associated with the poor response to chemotherapy on human osteosarcoma cells suggesting the key role of these proteins in bone cancer chemoresistance. [39]

On the other hand, clinical evidences demonstrate that FAK contributes to cell migration and invasion of several solid tumors partly through regulating expressions and activations of both MMP-2 and MMP-9**.** [40,41] In this sense, many scientific reports showed the importance to inhibit the FAK functions to block the activation of MMP-2 and MMP-9.[42,43] Our previous results demonstrated that **$VO(CQ)_2$** reduces the phosphorylation level of FAK Tyr 576/577 at 10 μM [11] and this effects could be , at least partly, may be involved in the lack of activities of MMP-2 and MMP-9.

2.6 Effect of $VO(CQ)_2$ on 3D cell migration

With the purpose to clarify and determine the antimetastatic effects of **$VO(CQ)_2$**, we evaluate their actions on cell migration in MG-63 multicellular spheroids.

Figure 8 show that the **$VO(CQ)_2$** inhibited cell migration properties of MG-63 multicellular spheroids in a concentration- manner response from 2.5 to 10 μM ($p < 0.01$). In this sense, at 2.5 μM, the compound decreases the cell migration on 44% compared to basal conditions whilst, at 10 μM, these values decreased until 67% ($p < 0.01$). In

Metallomics Accepted Manuscript

View Article Online
DOI: 10.1039/D0MT00176G

addition, the antimetastasic effects of $VO(CQ)_2$ are in accordance with the 2D cell migration (wound healing).

3. Conclusion

Novel oxidovanadium(IV) compounds with potential anticancer and antimetastatic properties currently require more intensive investigation since information obtained from the in vitro studies may allow vanadium drugs to enter the preclinical in vivo phase. Based on, we have thoroughly investigated the mode of interaction between FAK and the oxovanadium(IV)–clioquinol compound using computational platforms (docking and MD) and the anti-cell migration properties of this compound using 2D and 3D in vitro cell experiments.

We have investigated and reported herein for the first time the possible mechanism of inhibition of FAK by $VO(CQ)_2$ and the relationship with the antitumoral properties on a human osteosarcoma cell line (MG-63).

The results showed that $VO(CQ)_2$ is located near of the activation loop of the kinase domain and establishes interactions with residues in the ATP binding site. The most important residues that participate in the interaction are Ile428, Leu501, Cys502, Gly505, Glu506, Asn551, Leu553, Gly563, Asp564, and Leu567.

On the other hand, the compound reduced the cell migration on 2D and 3D human bone cancer cell models. Besides, $VO(CQ)_2$ significantly reduced the activity of MMP-2 and MMP-9 in a dose-dependent manner suggesting the directly relationship between FAK inhibition and the inactivation of MMPs.

Taken together, these results indicate that $VO(CQ)_2$ is a promising candidate with potential antimetastatic activity on osteosarcoma cells so it would be interesting to test this complex in further in vivo assays for cancer treatments.

4. Experimental

4.1 Preparation of the Molecular Systems

The simulations were based on a X-ray crystal structure FAK Domain Kinase (PDB: 4GU6). The preparation of receptor was done with Molprobity [44]. Water molecules and

Published on 14 October 2020. Downloaded by Auckland University of Technology on 10/26/2020 7:34:17 PM.

Metallomics Accepted Manuscript

View Article Online
DOI: 10.1039/D0MT00176G

Published on 14 October 2020. Downloaded by Auckland University of Technology on 10/26/2020 7:34:17 PM.

other ligands were removed. All Asp and Glu residues were considered to have a negative charge and all the Arg and Lys residues were considered to have a positive charge. Histidine tautomers were assigned following the hydrogen bonding pattern.

Three reference FAK inhibitor structures: **NVP-TAE226** [20], **PF-562,271** [21], and N-{3-[(5-Cyano-2-phenyl-1H-pyrrolo[2,3-b]pyridin-4-ylamino)-methyl]-pyridin-2-yl}-N-methyl-methanesulfonamide [22], referred to as **10N,** were obtained in complex with FAK from RCSB protein Data Bank (PDB), prepared with Avogadro molecular editor [45]. Finally, the structures were optimized to a gradient norm of <0.1 in the gas phase using PM7 [46] semiempirical method implemented in Molecular Orbital PACkage (MOPAC) program[47].

The structure of oxovanadium(IV) complex, **$VO(CQ)_2$**, was built with Avogadro [45], based on other experimental oxavanadium(IV) structures, and then optimized with Gaussian03 using B3LYP density functional [48] and 6-311+G(d,p) basis set [49], with default settings. The **$VO(CQ)_2$** calculated structure is available in Supplementary Material. Due to the lack of an experimental structure, a comparison was made with bis(2-methyl-8-quinolinolato)oxovanadium(IV) x-ray structure obtained by M. Shiro *et al* [50] (the most representative angles and bond length are shown in Table SM2).

4.2 Molecular Docking Studies

Molecular docking was carried out to find and score protein-ligand binding poses on FAK Kinase Domain with Autodock 4.2 [51]. To avoid biased results, initial coordinates of reference inhibitors were modified before docking, generating random positions and conformations. Protein and ligands were prepared with AutodockTools software, and ligands were docked using a flexible-ligand/rigid-receptor approach. A docking box with size 19.88 Å × 17.25 Å × 19.12 Å were centered on the ATP binding site, applying a space grid of 0.375 Å. The lowest pose energy of most populated cluster was selected after 100 cycles of running a Lamarckian genetic algorithm with a population size of 300, a maximum of 2.5 million energy evaluations, a maximum of 27000 generations, a mutation rate of 0.02, and crossover rate of 0.8. The results were clustered using a tolerance of 2.0 Å.

The post-docking analysis included visualization of the ligand-receptor complexes with Pymol [52] to analyze the potential interactions with the amino acid components of ATP

Metallomics Accepted Manuscript

View Article Online
DOI: 10.1039/D0MT00176G

binding site.

4.3 Molecular Dynamics (MD) Simulations

MD simulations were performed on poses of ligands in ATP site of FAK Kinase Domain resulting from molecular docking. The complexes have a positive net charge, chlorides anions were added as counterions with Leap module to achieve electroneutrality. The neutralized complexes were immersed in a box of TIP3P waters which extended up to 15 Å from the solute. Protein were described using the Amber14SB force field [53]. Ligands were described using the Generalized Amber Force Field (GAFF) [54] with charges derived from AM1-BCC, which were calculated with Antechamber module. Leap and Antechamber are included in the package AmberTools 16.0 [55]. In particular, **$VO(CQ)_2$** was modeled using the python-based metal center parameter builder, MCPB.py [56], also included in AmberTools 16.0. This software simplifies the process to obtain the metal site force-field parameters and charges, which were derived from QM calculations at 6-311+G(d,p) level of theory using Gaussian 03. Frequency calculations were also performed at the same level to approximate the force constants, using Seminario method, which is based on the Hessian matrix. In addition, it was observed during the DM trajectory that the structure does not undergo significant changes with respect to the optimized conformation with DFT.

All MD simulations were run using the NAMD 2.10 software [57]. The van der Waals interaction cutoff distances were set at 12 Å and long-range electrostatic forces were computed using the particle mesh Ewald summation method with a grid size set to 1.0 Å. The 1-4 contributions were multiplied by a factor of 0.83 to match the AMBER force field requirements. The system was subjected to 100000 minimization steps and heating from 0 to 300K. For all production simulations, constant temperature (300 K) was maintained using Langevin dynamics with a damping coefficient of 5 ps^{-1}, while pressure was kept constant at 1 atm through the Nosé-Hoover Langevin piston method with a decay period of 200 fs and a damping time constant of 100 fs. A time step of 1 fs was used along molecular mechanics. Bonds involving hydrogen atoms of waters were constrained using the SHAKE algorithm RMSD values were depicted as a line-style plot to determine the convergence and stability of simulations.

4.4 MM-GB/SA calculations

Published on 14 October 2020. Downloaded by Auckland University of Technology on 10/26/2020 7:34:17 PM.

Metallomics Accepted Manuscript

View Article Online
DOI: 10.1039/D0MT00176G

Reference inhibitors and **VO(CQ)$_2$** binding free energies with FAK Kinase Domain were computed using the MM-GB/SA method for all complexes, where the binding free energy is calculated as the difference between the bound and unbound states of protein and ligand [58].

The entropic changes upon binding were assumed constant. The solvation free energy was calculated using the generalized Born (GB) model implemented in MMPBSA.py module [59] igb=2 as selected model. The hydrophobic contribution was determined using the solvent-accessible surface area (SASA). The protein–ligand binding free energy was calculated using a single trajectory (for ligand, receptor and complex) based on 500 snapshots taken from the last 10 ns portion (20 ps interval) of the MD simulation trajectories. MMPBSA.py does not have the parameters for vanadium so it was necessary to include its radio. Based on trends in the included parameters of other elements, it was decided to use 1.2 Å as V radius. We observed that the effect of varying this value did not significantly affect the results, probably because the metal is little exposed to the solvent.

For the purpose of obtaining the detailed representation of interactions, free energy decomposition analysis was employed to decompose the total binding free energies into ligand–residue pairs. These calculations were performed using a pairwise energy decomposition scheme (idecomp option 3) also with the MMPBSA.py module. In this scheme, interactions are decomposed by specific residue pairs by including only those interactions in which one atom from each of the analyzed residues is participating, following the work of Miller et al [59]

4.5 Synthesis and identification of VO(CQ)$_2$

$VO(CQ)_2$ was synthesized according to previously reported results [29]. Briefly, clioquinol (0.61 g) was dissolved in 150 mL of warm ethanol. To this solution, 0.35 g of $VOSO_4$ 5H O mixed in 10 mL of hot ethanol was added dropwise. The solution became dark and the complex precipitated after stirring for a short while. After digestion for a short while over a water bath, it was filtered, washed with absolute ethanol and dried for 3 days at 60 °C. Anal. calc. for C18 H8 N2 O3 Cl2 I2 V C 31.91; H 1.18; N 4.14; V 7.54; exp. C 31.80; H 1.27; N 4.26; V 7.66.

Published on 14 October 2020. Downloaded by Auckland University of Technology on 10/26/2020 7:34:17 PM.

Metallomics Accepted Manuscript

View Article Online
DOI: 10.1039/D0MT00176G

The identification of the complex was done by Fourier-transform infrared spectroscopy (FTIR).

4.6 Preparation of $VO(CQ)_2$ solutions

Fresh stock solutions of the complex were prepared in Dimethyl sulfoxide (DMSO) at 20 mM and diluted according to the concentrations indicated in the legends of the figures. We used 0.5% as the maximum DMSO concentration in order to avoid the toxic effects of this solvent on the cells.

4.7 Cell line and growth conditions

Human osteosarcoma cell line (MG-63) was grown in Dulbecco's modified Eagle's medium (DMEM) containing 10% fetal bovine serum (FBS), 100 IU/mL penicillin and 100 µg/mL streptomycin at 37 °C in 5% CO_2 atmosphere. All cancer cell lines in a 75 cm^2 flask were grown until they reach 70–80% of confluence. Then, the cells were subcultured using TrypLE ™. For experiments, cells were grown in multi-well plates. Dulbecco's modified Eagle's médium (DMEM) and TrypLE ™ were purchased from Gibco (Gaithersburg, MD, USA), and fetal bovine serum (FBS) was purchased from Internegocios (Argentina). After 24 h the monolayers were washed with DMEM and were incubated under different conditions according to the experiments. Tissue culture materials were purchased from Corning (Princeton, NJ, USA).

4.8 Wound healing assay

Cells were grown in a 12 well cell culture plates with complete DMEM including 10% FBS, until 100% of confluence. The monolayer was scratched and washed with PBS to remove non-adherent cells. Then, the cells were treated with **$VO(CQ)_2$** (2.5 -10 µM) for 24 hours. After this time, the monolayer was washed with PBS and stained with Giemsa. Digital images were taken using an Olympus BX51 inverted microscope with a digital camera. The inhibition of cell migration was analyzed with ImageJ software. The percentage (%) of migration was calculated using the following formula: 100-(final area/initial area × 100%).

Published on 14 October 2020. Downloaded by Auckland University of Technology on 10/26/2020 7:34:17 PM.

Metallomics Accepted Manuscript

View Article Online
DOI: 10.1039/D0MT00176G

Published on 14 October 2020. Downloaded by Auckland University of Technology on 10/26/2020 7:34:17 PM.

4.9 Gelatin zymography

MMP-2 and MMP-9 activities were measured in supernatant of MG-63 cells treated with different concentrations (2.5 -10 µM) of **$VO(CQ)_2$** for 24 h.

Samples were separated in polyacrylamide gels with a concentration of 8% Acrylamide/Bisacrylamide, 0.1% SDS and a pH of 8.8, containing 1mg/ml of gelatin. Proteins were separated under a constant voltage of 100 V. After electrophoresis, gels were washed four times in Triton-X 100 for 15 min and incubated for 72 h at 37 °C in developing buffer consisting of 200 mM NaCl, 10 mM $CaCl_2$ and 50 mM Tris pH 7.5, in order to activate MMPs. After incubation, staining was performed with 0.5 mg/ml Coomassie Brilliant Blue R-250 in 10% acetic acid and 25% methanol for 1 h with gentle agitation, before being destained for 2 h in 8% acetic acid and 4% methanol.

Gels were photographed to enable densitometric analysis. MMP activity was determined by the intensity of the pale bands against the stained background and MMPs were identified by their molecular weights using ImageJ software.

4.10 Multicellular spheroids (MCS) formation

The development of MCS was achieved by the hanging drop technique with minor modifications [7]. The cell suspension was adjusted to a concentration of 2400 cells/mL. This concentration was selected to get 500 µm diameter spheroids at the beginning of the treatment with the compound. After 48 h, the compacted spheroids were transferred to an agar coated 96-well plate, and then, 200 µL of DMEM plus 10 % FBS were added to each well. The plate was cultured under the standard conditions for eight days, replacing 50 % of the culture media every 48 h for 1 week.

4.11 Migration assay in 3D MCS

The 3D MCS migration assay spheroids was achieved following indications reported by Ruiz et al [60].

After the time-point required for cell aggregation (72 h), the spheroids were transferred to agarose-coated 96-well plates (one droplet in one well) and cultured with 150 µl culture medium (size= 300 µm diameter). Then, spheroids were then transferred to a

Metallomics Accepted Manuscript

View Article Online
DOI: 10.1039/D0MT00176G

conventional 48-well plate and treated with different concentration of the complex. Spheroids were allowed to adhere, and images were obtained after 48h, using an inverted microscope. Effects of the compound were analysed by measuring the area covered by migration cells using ImageJ software.

Acknowledgments

This work was partly supported by UNLP (PPID X041), CONICET (PIP 0340), and ANPCyT (PICT 2016-1574,) from Argentina. IEL and MJL are members of the Carrera del Investigador, CONICET, Argentina. LMB and PQ have a fellowship from CONICET. EJB is an Emeritus Professor from National University of La Plata.

We gratefully acknowledge the support of NVIDIA Corporation with the donation of the Titan X Pascal GPU used for this research.

Conflict of interest

There are no conflicts to declare

References

1 N. FH, *Metal Ions in Biological Systems: Volume 31: Vanadium and its Role for Life*, CRC Press, 1995.

2 J. C. Pessoa, S. Etcheverry and D. Gambino, *Coord. Chem. Rev.*, 2015, **301–302**, 24–48.

3 C. S. Navara, A. Benyumov, A. Vassilev, R. K. Narla, P. Ghosh and F. M. Uckun, *Anticancer. Drugs*, 2001, **12**, 369–76.

4 R. K. Narla, Y. Dong, D. Klis and F. M. Uckun, *Clin. Cancer Res.*, 2001, **7**, 1094–101.

5 I. E. Leon, V. Porro, a. L. Di Virgilio, L. G. Naso, P. a M. Williams, M. Bollati-Fogolín and S. B. Etcheverry, *J. Biol. Inorg. Chem.*, 2014, **19**, 59–74.

6 A. Tesmar, D. Wyrzykowski, R. Kruszyński, K. Niska, I. Inkielewicz-Stępniak, J. Drzeżdżon, D. Jacewicz and L. Chmurzyński, *BioMetals*, 2017, **30**, 261–275.

7 I. E. León, J. F. Cadavid-Vargas, A. Resasco, F. Maschi, M. A. Ayala, C. Carbone and S. B. Etcheverry, *JBIC J. Biol. Inorg. Chem.*, 2016, **21**, 1009–1020.

Published on 14 October 2020. Downloaded by Auckland University of Technology on 10/26/2020 7:34:17 PM.

Metallomics Accepted Manuscript

View Article Online
DOI: 10.1039/D0MT00176G

Published on 14 October 2020. Downloaded by Auckland University of Technology on 10/26/2020 7:34:17 PM.

8 I. E. León, N. Butenko, a. L. Di Virgilio, C. I. Muglia, E. J. Baran, I. Cavaco and S. B. Etcheverry, *J. Inorg. Biochem.*, 2014, **134**, 106–117.

9 I. Leon, J. Cadavid-Vargas, A. Di Virgilio and S. Etcheverry, *Curr. Med. Chem.*, 2017, **24**, 112–148.

10 I. E. León, P. Díez, S. B. Etcheverry and M. Fuentes, *Metallomics*, 2016, **8**, 739–49.

11 I. E. León, P. Díez, E. J. Baran, S. B. Etcheverry and M. Fuentes, *Metallomics*, 2017, **9**, 891–901.

12 N. Pagano, J. Maksimoska, H. Bregman, D. S. Williams, R. D. Webster, F. Xue and E. Meggers, *Org. Biomol. Chem.*, 2007, **5**, 1218–27.

13 G. E. Atilla-Gokcumen, L. Di Costanzo and E. Meggers, *J. Biol. Inorg. Chem.*, 2011, **16**, 45–50.

14 L. Feng, Y. Geisselbrecht, S. Blanck, A. Wilbuer, G. E. Atilla-Gokcumen, P. Filippakopoulos, K. Kräling, M. A. Celik, K. Harms, J. Maksimoska, R. Marmorstein, G. Frenking, S. Knapp, L.-O. Essen and E. Meggers, *J. Am. Chem. Soc.*, 2011, **133**, 5976–5986.

15 J. Maksimoska, L. Feng, K. Harms, C. Yi, J. Kissil, R. Marmorstein and E. Meggers, *J. Am. Chem. Soc.*, 2008, **130**, 15764–5.

16 M. Luo, H. Fan, T. Nagy, H. Wei, C. Wang, S. Liu, M. S. Wicha and J.-L. Guan, *Cancer Res.*, 2009, **69**, 466–74.

17 V. M. Golubovskaya, *Front. Biosci. (Landmark Ed.*, 2014, **19**, 687–706.

18 G. W. McLean, E. Avizienyte and M. C. Frame, *Expert Opin. Pharmacother.*, 2003, **4**, 227–234.

19 F. J. Sulzmaier, C. Jean and D. D. Schlaepfer, *Nat. Rev. Cancer*, 2014, **14**, 598–610.

20 D. Lietha and M. J. Eck, *PLoS One*, 2008, **3**, e3800.

21 W. G. Roberts, E. Ung, P. Whalen, B. Cooper, C. Hulford, C. Autry, D. Richter, E. Emerson, J. Lin, J. Kath, K. Coleman, L. Yao, L. Martinez-Alsina, M. Lorenzen, M. Berliner, M. Luzzio, N. Patel, E. Schmitt, S. LaGreca, J. Jani, M. Wessel, E. Marr, M. Griffor and F. Vajdos, *Cancer Res.*, 2008, **68**, 1935–44.

22 T. Heinrich, J. Seenisamy, L. Emmanuvel, S. S. Kulkarni, J. Bomke, F. Rohdich, H. Greiner, C. Esdar, M. Krier, U. Grädler and D. Musil, *J. Med. Chem.*, 2013, **56**, 1160–70.

23 D. Lietha, X. Cai, D. F. J. Ceccarelli, Y. Li, M. D. Schaller and M. J. Eck, *Cell*,

Metallomics Accepted Manuscript

View Article Online
DOI: 10.1039/D0MT00176G

2007, **129**, 1177–87.

24 V. Oliveri and G. Vecchio, *Eur. J. Med. Chem.*, 2016, **120**, 252–274.

25 S. Mukherjee, T. E. Balius and R. C. Rizzo, *J. Chem. Inf. Model.*, 2010, **50**, 1986–2000.

26 K. Mena-Ulecia, W. Tiznado and J. Caballero, *PLoS One*, 2015, **10**, e0142774.

27 J.-Y. Zhan, J.-L. Zhang, Y. Wang, Y. Li, H.-X. Zhang and Q.-C. Zheng, *J. Biomol. Struct. Dyn.*, 2016, **34**, 2351–66.

28 V. Gabarra-Niecko, P. J. Keely and M. D. Schaller, *Biochem. J.*, 2002, **365**, 591–603.

29 A. C. Gonzalez-Baró and E. J. Baran, *Monatshefte Chemie Chem. Mon.*, 1997, **128**, 323–335.

30 C. R. Justus, N. Leffler, M. Ruiz-Echevarria and L. V Yang, *J. Vis. Exp.*, , DOI:10.3791/51046.

31 S. Mirjalili, M. Dejamfekr, A. Moshtaghian, M. Salehi, M. Behzad and A. Khaleghian, *Drug Res. (Stuttg).*, , DOI:10.1055/a-1235-5565.

32 G. Scalese, M. F. Mosquillo, S. Rostán, J. Castiglioni, I. Alho, L. Pérez, I. Correia, F. Marques, J. Costa Pessoa and D. Gambino, *J. Inorg. Biochem.*, 2017, **175**, 154–166.

33 M. S. Molinuevo, A. M. Cortizo and S. B. Etcheverry, *Cancer Chemother. Pharmacol.*, 2008, **61**, 767–73.

34 L. G. Naso, I. Badiola, J. Marquez Clavijo, M. Valcarcel, C. Salado, E. G. Ferrer and P. A. M. Williams, *Bioorganic Med. Chem.*, 2016, **24**, 6004–6011.

35 M. Egeblad and Z. Werb, *Nat. Rev. Cancer*, 2002, **2**, 161–174.

36 M. S. Benassi, G. Gamberi, G. Magagnoli, L. Molendini, P. Ragazzini, M. Merli, F. Chiesa, A. Balladelli, M. Manfrini, F. Bertoni, M. Mercuri and P. Picci, *Ann. Oncol. Off. J. Eur. Soc. Med. Oncol.*, 2001, **12**, 75–80.

37 J. E. Rundhaug, *Clin. Cancer Res.*, 2003, **9**, 551–4.

38 S. Petanidis, E. Kioseoglou, M. Hadzopoulou-Cladaras and A. Salifoglou, *Cancer Lett.*, 2013, **335**, 387–396.

39 P. Kunz, H. Sähr, B. Lehner, C. Fischer, E. Seebach and J. Fellenberg, *BMC Cancer*, 2016, **16**, 223.

40 Y. Jing, W. Liang, J. Liu, L. Zhang, J. Wei, Y. Zhu, J. Yang, K. Ji, Y. Zhang and Z. Huang, *Pathol. Res. Pract.*, , DOI:10.1016/j.prp.2019.152564.

41 J. S. Chen, X. H. Huang, Q. Wang, X. L. Chen, X. H. Fu, H. X. Tan, L. J. Zhang,

Published on 14 October 2020. Downloaded by Auckland University of Technology on 10/26/2020 7:34:17 PM.

Metallomics Accepted Manuscript

View Article Online
DOI: 10.1039/D0MT00176G

Published on 14 October 2020. Downloaded by Auckland University of Technology on 10/26/2020 7:34:17 PM.

W. Li and J. Bi, *Clin. Exp. Metastasis*, 2010, **27**, 71–82.

42 J. K. Woo, H. J. Jung, J. Y. Park, J. H. Kang, B. Il Lee, D. Y. Shin, C. W. Nho, S. Y. Cho, J. K. Seong and S. H. Oh, *Oncotarget*, 2017, **8**, 57058–57071.

43 Q. Jiang, Y. Pan, Y. Cheng, H. Li, D. Liu and H. Li, *Oncol. Rep.*, 2016, **36**, 253–262.

44 V. B. Chen, W. B. Arendall, J. J. Headd, D. A. Keedy, R. M. Immormino, G. J. Kapral, L. W. Murray, J. S. Richardson and D. C. Richardson, *Acta Crystallogr. D. Biol. Crystallogr.*, 2010, **66**, 12–21.

45 M. D. Hanwell, D. E. Curtis, D. C. Lonie, T. Vandermeersch, E. Zurek and G. R. Hutchison, *J. Cheminform.*, 2012, **4**, 17.

46 J. J. P. Stewart, *J. Mol. Model.*, 2013, **19**, 1–32.

47 J. J. P. Stewart, *J. Comput. Aided. Mol. Des.*, 1990, **4**, 1–103.

48 C. Lee, W. Yang and R. G. Parr, *Phys. Rev. B*, 1988, **37**, 785–789.

49 P. J. Hay and W. R. Wadt, *J. Chem. Phys.*, 1985, **82**, 299–310.

50 M. Shiro and Q. Fernando, *J. Chem. Soc. D Chem. Commun.*, 1971, 63–64.

51 G. M. Morris, R. Huey, W. Lindstrom, M. F. Sanner, R. K. Belew, D. S. Goodsell and A. J. Olson, *J. Comput. Chem.*, 2009, **30**, 2785–91.

52 DeLano, W.L. (2002) The PyMOL Molecular Graphics System. Delano Scientific, San Carlos. - References - Scientific Research Publishing, https://www.scirp.org/(S(vtj3fa45qm1ean45vvffcz55))/reference/ReferencesPapers.aspx?ReferenceID=1958992, (accessed 29 July 2020).

53 J. A. Maier, C. Martinez, K. Kasavajhala, L. Wickstrom, K. E. Hauser and C. Simmerling, *J. Chem. Theory Comput.*, 2015, **11**, 3696–3713.

54 J. Wang, W. Wang, P. A. Kollman and D. A. Case, *J. Mol. Graph. Model.*, 2006, **25**, 247–260.

55 D. A. Case, T. E. Cheatham, T. Darden, H. Gohlke, R. Luo, K. M. Merz, A. Onufriev, C. Simmerling, B. Wang and R. J. Woods, *J. Comput. Chem.*, 2005, 26, 1668–1688.

56 P. Li and K. M. Merz, *J. Chem. Inf. Model.*, 2016, **56**, 599–604.

57 J. C. Phillips, R. Braun, W. Wang, J. Gumbart, E. Tajkhorshid, E. Villa, C. Chipot, R. D. Skeel, L. Kalé and K. Schulten, *J. Comput. Chem.*, 2005, **26**, 1781–802.

58 Y. N. Vorobjev and J. Hermans, *Biophys. Chem.*, 1999, **78**, 195–205.

59 B. R. Miller, T. D. McGee, J. M. Swails, N. Homeyer, H. Gohlke and A. E. Roitberg, *J. Chem. Theory Comput.*, 2012, **8**, 3314–21.

Metallomics Accepted Manuscript

60 M. C. Ruiz, J. Kljun, I. Turel, A. L. Di Virgilio and I. E. León, *Metallomics*, 2019, **11**, 666–675.

View Article Online
DOI: 10.1039/D0MT00176G

Published on 14 October 2020. Downloaded by Auckland University of Technology on 10/26/2020 7:34:17 PM.

Metallomics Accepted Manuscript

View Article Online
DOI: 10.1039/D0MT00176G

Published on 14 October 2020. Downloaded by Auckland University of Technology on 10/26/2020 7:34:17 PM.

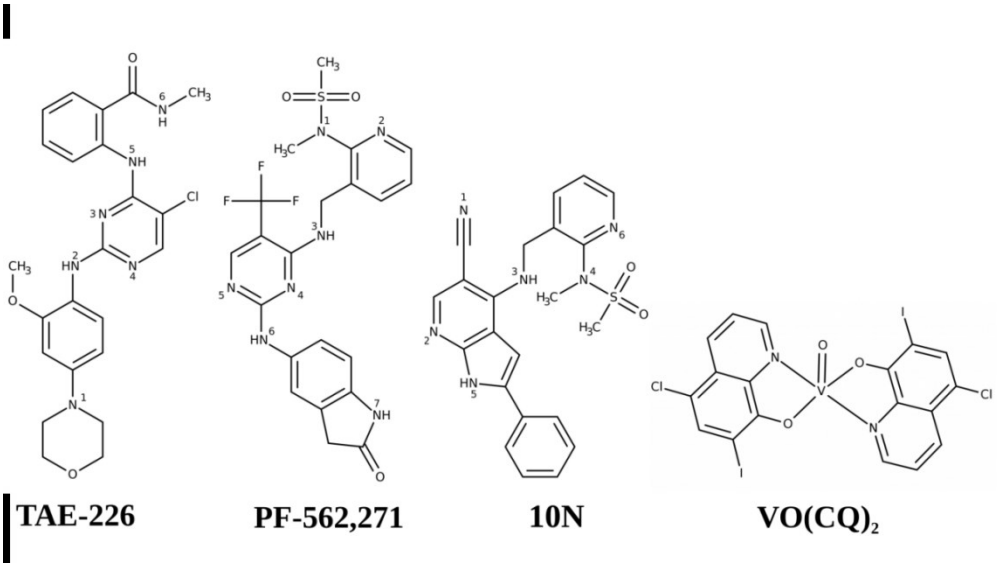

Figure 1. Structures of coordination complex VO(CQ)2 and inhibitors used in redocking study.

Metallomics Accepted Manuscript

View Article Online
DOI: 10.1039/D0MT00176G

Published on 14 October 2020. Downloaded by Auckland University of Technology on 10/26/2020 7:34:17 PM.

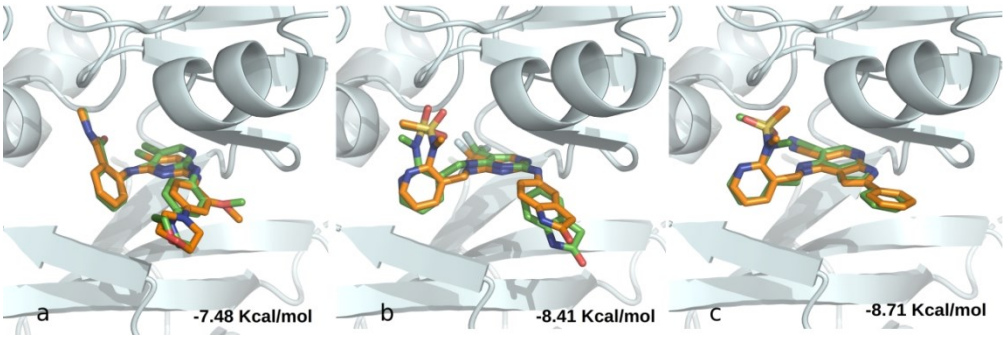

Figure 2. Redocking of crystallized inhibitors with FAK in ATP binding site. Comparison of the docked structures (green) with X-ray reference structures (orange). (a) TAE-226 (b) PF-562,271 (c) 10N.

Metallomics Accepted Manuscript

View Article Online
DOI: 10.1039/D0MT00176G

Published on 14 October 2020. Downloaded by Auckland University of Technology on 10/26/2020 7:34:17 PM.

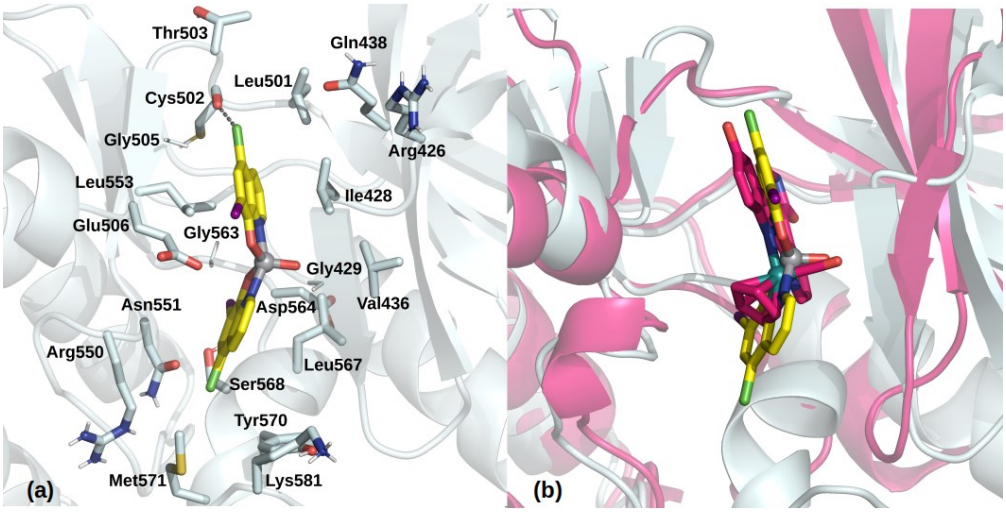

Figure 3. (a) VO(CQ)2 localization in ATP binding site and (b) comparison with ruthenium complex position in Glycogen Synthase Kinase 3 [PDB Id 3M1S].

Metallomics Accepted Manuscript

View Article Online
DOI: 10.1039/D0MT00176G

Published on 14 October 2020. Downloaded by Auckland University of Technology on 10/26/2020 2:34:17 PM.

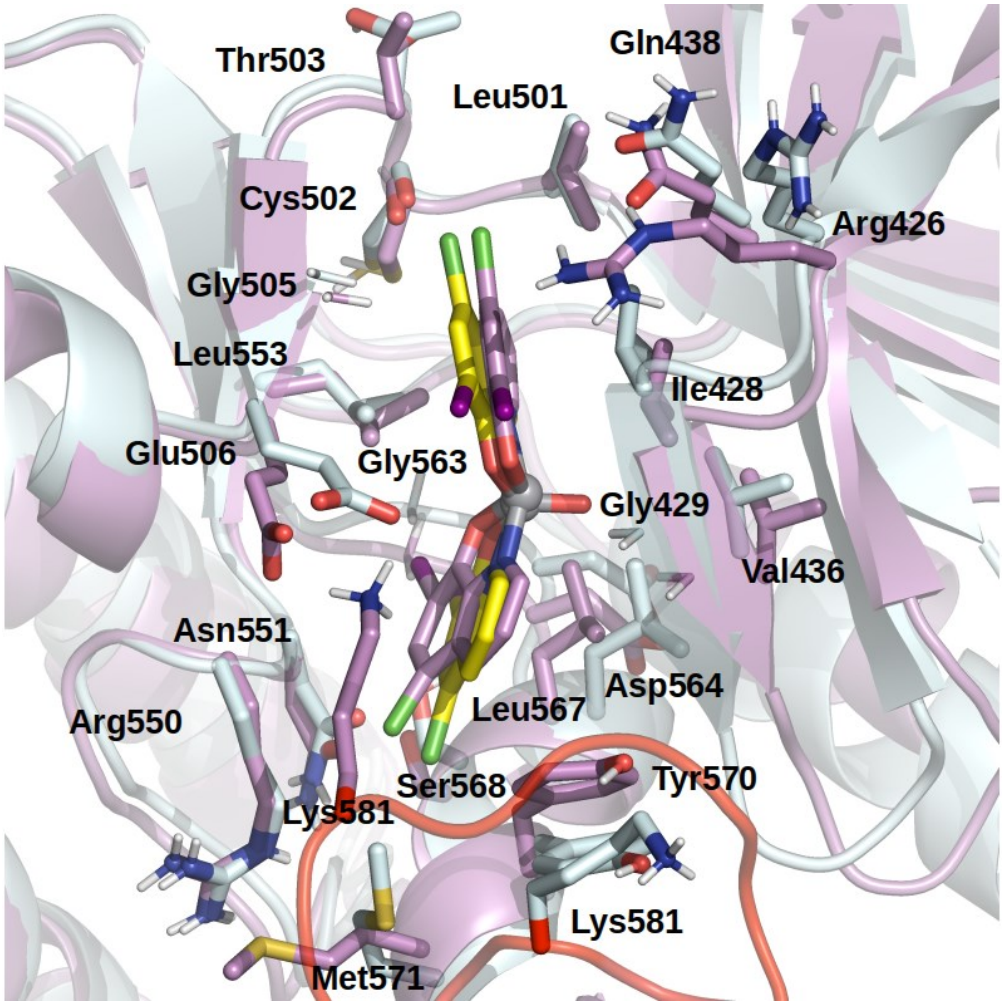

Figure 4. Binding mode of VO(CQ)2 in ATP binding site after 40ns MD simulation (shown in violet) and comparison with the docking results (protein structure and ligand pose are shown in white and yellow, respectively). The activation loop is highlighted in red for both cases.

Metallomics Accepted Manuscript

View Article Online
DOI: 10.1039/D0MT00176G

Published on 14 October 2020. Downloaded by Auckland University of Technology on 10/26/2020 2:34:17 PM.

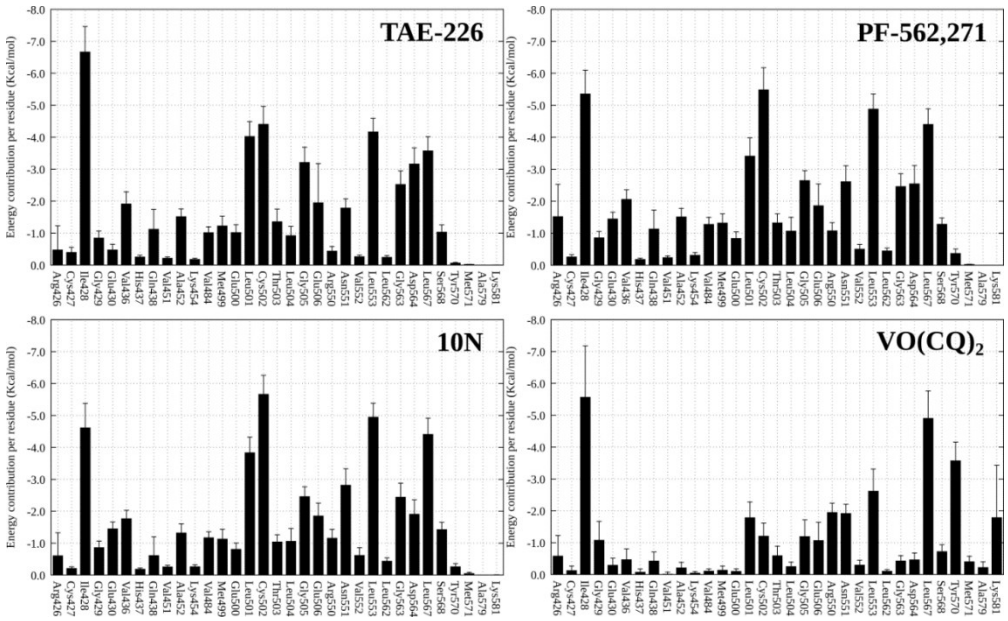

Figure 5. Plot of MM-GB/SA binding free energy contribution per residue for reference inhibitors and VO(CQ)2, calculated with MMPBSA.py.

Metallomics Accepted Manuscript

View Article Online
DOI: 10.1039/D0MT00176G

Published on 14 October 2020. Downloaded by Auckland University of Technology on 10/26/2020 7:34:17 PM.

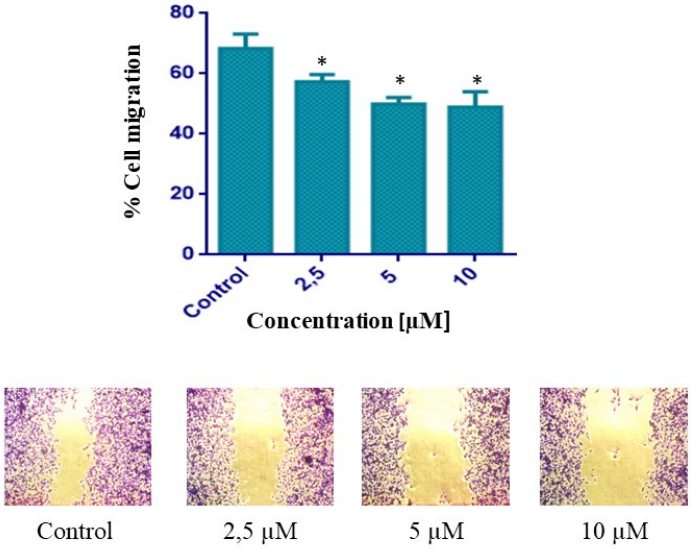

Figure 6. Wound healing assay on MG-63 cells after 24 h of incubation with 2.5-10 µM of VO(CQ)2. * p< 0.01 differences between control and treatment with compounds.

254x190mm (96 x 96 DPI)

Metallomics Accepted Manuscript

View Article Online
DOI: 10.1039/D0MT00176G

Published on 14 October 2020. Downloaded by Auckland University of Technology on 10/26/2020 2:34:17 PM.

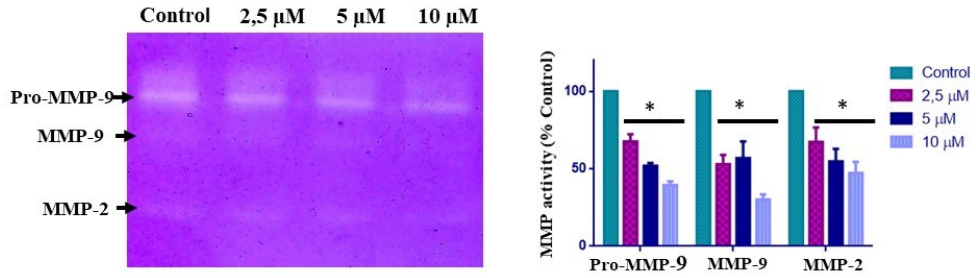

Figure 7. Effect of complex VO(CQ)2 on MMP2 and MMP9 activity on MG-63 cells after 24 h of incubation with VO(CQ)2 (2.5-10 µM). %"*p<0.01 differences between control and treatment, %"

Metallomics Accepted Manuscript

View Article Online
DOI: 10.1039/D0MT00176G

Published on 14 October 2020. Downloaded by Auckland University of Technology on 10/26/2020 2:34:17 PM.

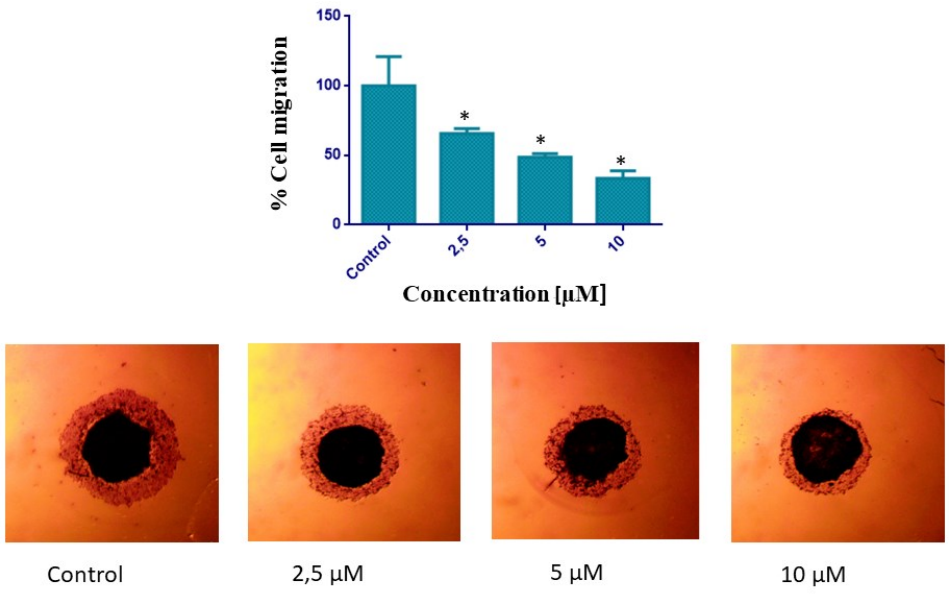

Figure 8. Effect of complex VO(CQ)2 on cell spreading of 3D MG-63 spheroids.
*p<0.01 differences between control and treatment.

254x190mm (96 x 96 DPI)

Metallomics Accepted Manuscript